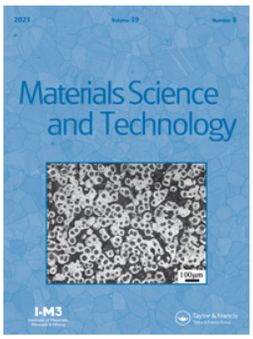

Materials Science and Technology

ISSN: (Print) (Online) Journal homepage: https://www.tandfonline.com/loi/ymst20

Modelling deformation-induced martensite transformation in high-carbon steels

Adriel Wong, Vikram Bedekar, Rohit Voothaluru & Enrique Galindo-Nava

To cite this article: Adriel Wong, Vikram Bedekar, Rohit Voothaluru & Enrique Galindo-Nava (2023): Modelling deformation-induced martensite transformation in high-carbon steels, Materials Science and Technology, DOI: 10.1080/02670836.2023.2187983

To link to this article: https://doi.org/10.1080/02670836.2023.2187983

Published online: 23 Mar 2023.

MATERIALS SCIENCE AND TECHNOLOGY
https://doi.org/10.1080/02670836.2023.2187983

I·M3 Institute of Materials, Minerals & Mining
Taylor & Francis Taylor & Francis Group

Modelling deformation-induced martensite transformation in high-carbon steels

Adriel Wong[a], Vikram Bedekar[b], Rohit Voothaluru[b] and Enrique Galindo-Nava[a,c]

[a]Department of Materials Science and Metallurgy, University of Cambridge, Cambridge, UK; [b]Materials Science Research and Development, Timken World Headquarters, North Canton, OH, USA; [c]Department of Mechanical Engineering, University College London, London, UK

ABSTRACT

The transformation behaviour of retained austenite in steels is known to differ according to chemical composition and other microstructural attributes. Earlier research indicated that austenite in high-carbon steels transforms into martensite only when the applied stress exceeds a critical value, contrary to low-carbon steels where transformation occurs in the early stages of deformation. Although transformation models have been proposed, most are optimised for low-carbon steels. Here, we propose physics-based models applied to high-carbon steels to overcome previous limitations. The models have fewer free parameters (4) compared to previous approaches (6), exhibiting improvements in the numerical and physical interpretation of the austenite transformation process. We envision the use of these models as tools for alloy design, also highlighting their scientific and technological value.

ARTICLE HISTORY
Received 13 October 2022
Revised 28 February 2023
Accepted 1 March 2023

KEYWORDS
Retained austenite; mechanical stability; deformation-induced; martensite transformation; kinetics; high-carbon steel

Introduction

The presence of retained austenite in steel has implications for its mechanical performance. For example, while retained austenite is reported to enhance the rolling contact fatigue life of bearings [1,2], excessive amounts can compromise its dimensional stability [3]. The opposing effects of retained austenite and its implications for bearing steels have been reviewed by Sidoroff et al. [3].

In a study on the mechanical stability of retained austenite in carburised bearing steels, Bedekar et al. [4] reported the onset of retained austenite transformation into martensite at a critical stress close to the yield point; retained austenite remained stable in the elastic deformation regime. Similar observations were reported in through-hardened steels [5–7]. In contrast, retained austenite in transformation-induced plasticity (TRIP) steels transforms into martensite almost immediately upon loading [8].

The mechanical stability (or kinematic stability) and transformation kinetics of retained austenite have been modelled in several investigations [4,7,9]. These studies employed crystal plasticity finite element models informed by experimental measurements of the transformed amounts of retained austenite. While micromechanical models can simulate the material response in detail, their implementation is complex and requires significant computational resources. Analytical models are simpler to implement, although their dependence on empirical data limits their range of applicability.

Haidemenopoulos et al. [10] developed an analytical model for calculating the critical stress required to transform retained austenite into martensite in a low-carbon steel; the model considers the effect of austenite chemical composition, size, and stress state. The critical stress is calculated to determine the M_s^σ temperature, which is an indicator of retained austenite mechanical stability. The application of this model has been demonstrated for low-carbon TRIP [11], quench-and-partition (QP) [12], and Fe-Ni-Co steels [13]. Therefore, it serves as a starting point in the present work.

Models that describe the kinetics of deformation-induced martensite transformation have been developed by previous authors [14–16]. Since these models are fitted to experimental data that are primarily from low-carbon steels, their direct application to high-carbon steels may lead to poor predictions of the transformation progress. This is because the effect of increased carbon concentration on the factors controlling austenite stability is not considered.

For example, the critical driving force to initiate martensite transformation increases with carbon concentration, which leads to the enhanced thermodynamic stability of retained austenite. The effect of carbon concentration also intrinsically affects the influence of austenite morphology [17] and the strength of the martensite matrix [18], where the latter influences the degree of stress–strain partitioning between austenite and martensite [19].

CONTACT Enrique Galindo-Nava e.galindo-nava@ucl.ac.uk Department of Materials Science and Metallurgy, University of Cambridge, Cambridge CB3 0FS, UK; Department of Mechanical Engineering, University College London, Torrington Place, London WC1E 7JE, UK

Table 1. Chemical compositions of the quench-and-tempered bearing steels used for model development. The asterisk (∗) represents the initial carbon content before carburisation. C_γ is shown beside the carbon content, and iron forms the balance of the respective compositions.

	Chemical composition / wt-%									
Steel	C	Mn	Si	Cr	Ni	Mo	*P*	S	Cu	Al
8620 [4]	0.2∗ (0.987)	1.43	0.32	0.74	0.28	0.09				
4320 [4]	0.2∗ (0.994)	0.78	0.33	0.64	1.6	0.22				
3310 [4]	0.1∗ (0.799)	0.45	0.26	1.51	3.39	0.06				
A485-M1 [5]	1.0 (0.813)	1.09	0.6	1.06	0.11		0.013	0.012		
52100-QT [6]	1.005 (0.800)	0.32	0.27	1.46	0.1				0.19	0.024

The aim of this work was to develop equations that model the critical stress and progress of deformation-induced martensite transformation in high-carbon steels. The equation developed by Haidemenopoulos et al. [10] was adapted to calculate the critical stress for martensite transformation in high-carbon steels. The critical stress was employed in an equation that calculates the transformed amount of retained austenite with applied stress. Both equations were validated with experimental data from bearing steels. A parametric analysis was conducted to study the limits of the critical stress equation, followed by examples illustrating the application of both equations in alloy design.

Material information

The equations were developed based on the experimental data for bearing steels reported in [4–7]. The chemical compositions of the bearing steels are shown in Table 1. The steels are labelled according to their original designations, and the heat treatments for these steels (known as 'quench-and-tempered steels' hereafter) are described in the respective works [4–7]. Their microstructures consist of martensite, retained austenite, and unreported amounts of carbide. The amount of carbides in the samples was noted to be small. Hence, carbides are not considered in the following calculations.

The carbon content in retained austenite (C_γ) before mechanical loading is shown beside the nominal carbon content of the respective steels. C_γ is normally estimated from equations relating the lattice parameter of retained austenite, a_γ, to the chemical composition. It is acknowledged that the C_γ could be affected by the effects of auto-tempering and accommodation stress induced by martensitic transformation on a_γ. However, measurements of the actual C_γ were not reported in the respective works [4–7], nor the cooling rates to determine possible auto-tempering effects. Given such limitations in the information, C_γ is estimated from composition-dependent lattice parameter equations.

Since the equations for evaluating C_γ are different in the respectively noted works, C_γ is derived based on the following expression to ensure consistency in calculations [6]:

$$a_\gamma = 3.556 + 0.0453x_C + 0.00095x_{Mn} + 0.056x_{Al} + 0.0006x_{Cr} + 0.0015x_{Cu} - 0.0002x_{Ni}, \quad (1)$$

where a_γ is the measured austenite lattice parameter in Å and x_i is the concentration of the alloying element in wt-%. The value for C_γ is derived from x_C (i.e. $C_\gamma = x_C$) and the concentrations of the other elements follow the bulk composition.

In the work of Foster et al. [6], the original C_γ for the 52100-QT steel was reported to be 0.593 wt-%C, which is much lower than expected. The C_γ for a 52100 steel has been reported to be 0.86 wt-%C [20] after undergoing heat treatment similar to the method employed by Foster et al. [6]. Therefore, the C_γ of 52100-QT steel in Table 1 is taken as 0.8 wt-%C for calculation purposes. It is also noted that the C_γ calculated for other steels mentioned in this work (including those in Tables 1 and 6) is close to the values quoted in the respective works [4–7].

Description of the critical stress model

Derivation of the critical stress model

Referring to the work of Haidemenopoulos et al. [10], the derivation of the critical stress model is presented in this section. The modifications made to adapt the original model [10] to high-carbon steels are presented in subsequent sections.

In stress-assisted martensite nucleation, the martensite nucleates at pre-existing sites within the parent austenite grain, which are the same nucleation sites where transformation under quenching occurs [21,22]. The applied stress influences the transformation kinetics by changing the potency distribution of these nucleation sites. This distribution can be described by a model of heterogeneous martensitic nucleation developed by Olson and Cohen [23,24].

The potency of a martensitic nucleation site, n, is represented by the thickness of the nucleus (in terms of the number of crystal planes) that is derived from the disassociation of existing defects. The critical n at a given thermodynamic driving force per unit volume is [10]:

$$n = -\frac{2 \cdot \gamma_s/\rho}{\Delta G_{Chem} + E_{Str} + W_F}, \quad (2)$$

where γ_s is the nucleus specific interfacial energy (J m^{-2}), ρ is the density of atoms in the fault plane (mol

m^{-2}), ΔG_{Chem} is the chemical driving force for martensitic transformation (J mol^{-1}), E_{Str} is the elastic strain energy (J mol^{-1}), and W_F is the frictional work of interfacial motion (J mol^{-1}).

When an external stress is applied, a mechanical driving force, ΔG_{Mech} (J mol^{-1}), is added to ΔG_{Chem} in Equation (2) to give the total driving force as:

$$\Delta G_{Total} = \Delta G_{Chem} + \Delta G_{Mech}. \quad (3)$$

ΔG_{Mech} varies with applied stress, σ (in MPa), according to:

$$\Delta G_{Mech} = \sigma \left(\frac{\partial \Delta G}{\partial \sigma} \right), \quad (4)$$

where $\frac{\partial \Delta G}{\partial \sigma}$ (J mol^{-1} MPa^{-1}) represents the stress state of the transforming plate [25].

Based on Equation (2), Cohen and Olson [26] derived the number density of operational nucleation sites N_v as:

$$N_v = N_v^0 \exp(-\alpha n), \quad (5)$$

where N_v^0 is the total number density of nucleation sites of all potencies (m^{-3}) and α is the dimensionless shape factor of the potency distribution [21].

For an austenite particle with volume V_p (m^3), the fraction of particles that will transform into martensite (f) via sites of potency with density N_v (m^{-3}) is equal to the probability of finding at least one nucleation site in the particle, assuming the austenite particle transforms into martensite in a single nucleation event [13]. This probability is given as [26]:

$$f = 1 - \exp(-N_v V_p). \quad (6)$$

Combining Equations (2)–(6), the critical stress at which martensite transformation initiates, σ_C (in MPa), can be expressed as:

$$\sigma_C = \frac{1}{\left(\frac{\partial \Delta G}{\partial \sigma}\right)} \cdot \left\{ \frac{2\alpha \cdot \gamma_s/\rho}{\ln\left[-\frac{\ln(1-f)}{N_v^0 \cdot V_p}\right]} - \Delta G_{Chem} - E_{Str} - W_F \right\}. \quad (7)$$

Equation (7) is the critical stress model that was originally developed by Haidemenopoulos et al. [10]. Equation (7) has four fixed parameters (γ_s, ρ, f, and E_{Str}) and six free parameters ($\left(\frac{\partial \Delta G}{\partial \sigma}\right)^{GH}$, α^{GH}, $(N_v^0)^{GH}$, V_p^{GH}, ΔG_{Chem}^{GH}, and W_F^{GH}). A list of symbols used in the present work and their definitions is shown in Table 2.

Table 2. List of symbols in the present work.

C_γ	Carbon content in retained austenite
a_γ	Lattice parameter of retained austenite
x_i	Concentration of alloying element in wt-%
n	Potency of a martensitic nucleation site
γ_s	Nucleus specific interfacial energy
ρ	Density of atoms in the fault plane
ΔG_{Chem}	Chemical driving force for martensitic transformation
E_{Str}	Elastic strain energy
W_F	Frictional work of interfacial motion
ΔG_{Mech}	Mechanical driving force for martensitic transformation
ΔG_{Total}	total driving force for martensitic transformation
$\frac{\partial \Delta G}{\partial \sigma}$	Stress state of transforming martensite plate
N_v	Number density of nucleation sites
N_v^0	Total number of nucleation sites of all potencies
α	Shape factor of potency distribution
V_p	Austenite particle volume
f	Fraction of particles to transform into martensite
σ	Applied stress
σ_C	Critical stress for the initiation of martensite transformation
V_γ^0	Initial volume fraction of retained austenite before mechanical loading
V_γ	Volume fraction of retained austenite

Calculation of parameters in Equation (7)

Equation (7) has been implemented to estimate the σ_C for the quench-and-tempered steels investigated. Details of the calculation using Equation (7) are presented in this section. For clarity, the parameters calculated using equations in the work of Haidemenopoulos et al. [10] are denoted with the superscript 'GH'; the latter represents the author's initials (e.g. ΔG_{Chem}^{GH}).

According to Haidemenopoulos et al. [10], ΔG_{Chem}^{GH} (J mol^{-1}) is calculated using the following linear expression:

$$\Delta G_{Chem}^{GH} = -5157.3 + 57979\psi_C - 37.353\psi_C T + 8.28T, \quad (8)$$

where ψ_C is the mole fraction of carbon in austenite and T is the temperature in degrees Celsius.

The parameter $\frac{\partial \Delta G}{\partial \sigma}^{GH}$ (in J mol^{-1} MPa^{-1}) is calculated according to the expression [10]:

$$\frac{\partial \Delta G}{\partial \sigma}^{GH} = -0.715 - 0.3206\left(\frac{\sigma_h}{\bar{\sigma}}\right), \quad (9)$$

where $\left(\frac{\sigma_h}{\bar{\sigma}}\right)$ is $-1/3$ for uniaxial compression, 1/3 for uniaxial tension and 0 for pure shear.

The frictional work of interfacial motion is expressed as a function of carbon concentration since it was assumed that carbon has the highest contribution to the frictional work [10]. The parameter W_F^{GH} (in J mol^{-1}) is calculated according to the expression [10]:

$$W_F^{GH} = 1.31 \times 10^4 \psi_C^{2/3}. \quad (10)$$

The parameter values for implementing Equation (7) are summarised in Table 3.

Modified critical stress model

The modifications made to adapt Equation (7) for calculating the σ_C of high-carbon quench-and-tempered steels are presented in this section.

In the earlier works of Haidemenopoulos et al. [11,13], the value for N_v^0 was estimated to be 2×10^{17}

Table 3. Model parameters for the implementation of Equation (7). Steel designations are included next to the values of ΔG_{Chem}^{GH} and W_F^{GH}.

Parameter	Parameter values in Equation (7)
$\left(\frac{\partial \Delta G}{\partial \sigma}\right)^{GH}$, in J mol^{-1} MPa^{-1}	−0.822
α^{GH}	0.866
$\gamma_{s'}$ in J m^{-2}	0.15
ρ, in mol m^{-2}	3×10^{-5}
f	0.01
$(N_v^0)^{GH}$, in m^{-3}	2×10^{17}
V_p^{GH}, in m^3	5.55×10^{-19}
$E_{Str'}$ in J mol^{-1}	500
$\Delta G_{Chem'}^{GH}$ in J mol^{-1}	−2465 (8620) −2444 (4320) −2929 (3310) −2905 (A485-M1) −2931 (52100-QT)
W_F^{GH}, in J mol^{-1}	1636 (8620) 1645 (4320) 1429 (3310) 1441 (A485-M1) 1429 (52100-QT)

m^{-3}. This value is derived from the work of Cohen et al. [26,27], which is based on fitting Equations (2) and (5) to the experimental data from Cech and Turnbull's small particle experiments which involved using a Fe-30Ni wt-% steel [28]. However, N_v^0 was found to be in the order of 1.5–4 $\times 10^{17}$ m^{-3} when fitted to experimental data from TRIP steels [21].

Similarly, the austenite particle volume, V_p, is not a constant value since it could be influenced by the type of steel and heat treatment employed. For instance, V_p has been reported to be 5.55×10^{-19} m^3 for a 4340 steel [10] and 4.18×10^{-18} m^3 for a TRIP steel [21]. The latter is based on TEM measurements of austenite particles with a mean radius of R = 1 µm [29], in which a spherical volume has been assumed for simplicity. In another work [30], V_p is found to be in the order of 10^{-20} m^3 based on an undeformed austenite particle diameter of 0.35 µm.

These reports show that the determination of V_p depends on the measured austenite particle size. While the dispersed austenite particles in the works of Haidemenopoulos et al. [10,21] are assumed to be spherical, this assumption cannot be applied to steels in the current work because the morphology of retained austenite was reported to appear as complex, heterogeneous, and interconnected in a tempered microstructure [4]. The size of retained austenite grains in tempered microstructures is also rarely reported, so any assumptions based on steels of other microstructures could lead to inaccurate calculations of σ_C.

The determination of N_v^0 and V_p is challenging given that they are material-dependent and require experimental measurements that cannot be obtained easily. An easier approach is to consider the product of these parameters $(N_v^0 \cdot V_p)$ as equivalent to the initial retained austenite volume fraction before mechanical loading, V_γ^0. By multiplying N_v^0 ($\sim \times 10^{17}$ m^{-3}) with V_p ($\sim \times 10^{-18}$ m^3), the product is a dimensionless quantity ($\sim \times 10^{-1}$) with a magnitude that is within the order of typical retained austenite volume fractions.

A similar approach was previously taken by Haidemenopoulos et al. in which the size effect of austenite particles is expressed as a scaled radius $(N_v^0 \cdot V_p)^{1/3}$ [13]. While the effects of N_v^0 and V_p are not explicitly considered in the modified equation, the advantage of condensing these effects into the V_γ^0 term is that V_γ^0 can be easily measured with conventional experimental methods such as XRD.

The calculation of ΔG_{Chem} for the quench-and-tempered steels using Equation (8) leads to an inaccurate calculation of σ_C. This is because Equation (8) is not valid for the composition range of the high-carbon steels investigated. The absence of concentration terms that account for other elements that can affect the driving force (e.g. nickel, manganese) is another limiting aspect for the application of Equation (8) in the present work.

Nowadays, it is convenient to calculate the Gibbs free energy with thermodynamic software. ΔG_{Chem} is calculated using Thermo-Calc software with the TCFE 8.1 database [31] in this study. For the present calculations, the chemical composition of retained austenite follows the composition of the respective steels in Table 1, where $C_\gamma = x_C$ after the evaluation of x_C from Equation (1). While it is acknowledged that C_γ can vary locally with different retained austenite grains, especially in carburised specimens, to simplify the calculations the current work assumes that C_γ is uniform across the microstructure. Since the quench-and-tempered steels were tested at room temperature, a temperature of 20°C was used in the thermodynamic calculations.

In initial calculations of σ_C for the quench-and-tempered high-carbon steels, the σ_C values calculated with Equation (7) were significantly higher than the experimental values (see Table 5). Since ΔG_{Chem} and W_F in Equation (7) are the terms that directly vary with chemical composition, the overestimation of σ_C is likely caused by inaccurate values of ΔG_{Chem} and W_F.

Because martensite transformation occurs via the movement of a glissile interface, the transformation can be suppressed by microstructural features that obstruct the mobility of the interfacial dislocations. The composition dependence of W_F arises from the fact that the resistance to dislocation motion was found to vary with solute concentration [32].

The limitations of a composition-based expression for W_F (i.e. Equation (10)) are similar to those described for ΔG_{Chem} earlier. Haidemenopoulos et al. previously expressed W_F as a function of carbon and manganese in [11], and nickel in [13]. While these linear expressions might be valid for low-carbon steels or those with simple alloying systems, they are not directly applicable to the present steels. This is because

Table 4. Model parameters for the implementation of Equation (11).

Parameter	Parameter values in Equation (11)
$\left(\frac{\partial \Delta G}{\partial \sigma}\right)^{AW}$, in J mol^{-1} MPa^{-1}	−0.86
α^{AW}	0.7899
γ_s, in J m^{-2}	0.15
ρ, in mol m^{-2}	3×10^{-5}
f	0.01
E_{Str}, in J mol^{-1}	500
ΔG^{AW}_{Chem}, in J mol^{-1}	−2214 (8620) −2150 (4320) −2090 (3310) −2623 (A485-M1) −2772 (52100-QT)
V^0_γ	0.43 (8620) 0.39 (4320) 0.31 (3310) 0.18 (A485-M1) 0.13 (52100-QT)

Table 5. The measured and calculated σ_C for the quench-and-tempered steels.

		Calculated σ_C/MPa	
Steel	Measured σ_C MPa	Equation (7), original model	Equation (11), modified model
8620	441	3987	453
4320	592	4023	592
3310	785	3170	830
A485-M1	1058	3214	715
52100-QT	1140	3168	946

Table 6. Material parameters, measured and calculated σ_C for steels with alternative microstructures.

Steel	V^0_γ	C_γ wt-%	ΔG^{AW}_{Chem} J mol^{-1}	Measured σ_C MPa	Calculated σ_C, Equation (11) MPa
A485-B1	0.18	0.930	−2345	722	1057
A485-B2	0.09	1.016	−2145	1436	2257
52100-B220	0.16	0.651	−3130	700	261
52100-B240	0.14	0.757	−2874	901	765
52100-B260	0.09	0.852	−2650	1070	1802
52100-QP220	0.20	0.727	−2946	731	248
52100-QP240	0.13	0.808	−2753	830	1001

the validity of the W_F expressions developed in [11,13] and [10] does not cover the composition of multicomponent high-carbon steels such as those in the present investigation. Attempts have been made to apply the W_F expression developed by Ghosh and Olson [32] (which considers multicomponent steel systems) in Equation (7) to calculate σ_C. However, the differences between the calculated and experimental σ_C values were significant, possibly due to errors that arise from limiting assumptions in the W_F expression developed by Ghosh and Olson [32].

In subsequent calculations using the modified critical stress model, where $N^0_v \cdot V_p$ is replaced with V^0_γ, it was found that reasonable values of σ_C can be obtained without including W_F in the calculations (see Table 5). It is acknowledged that the exclusion of W_F might indicate that the effect of alloying elements in impeding the mobility of the martensitic interface is not considered explicitly in the modified critical stress model.

However, the numerical contribution of W_F to the energy balance is likely to be incorporated in the $\frac{2\alpha \cdot \gamma_s/\rho}{\ln\left[-\frac{\ln(1-f)}{V^0_\gamma}\right]}$ term, such that the net difference between ΔG_{Chem} with $\frac{2\alpha \cdot \gamma_s/\rho}{\ln\left[-\frac{\ln(1-f)}{N^0_v \cdot V_p}\right]}$ and E_{Str} results in σ_C calculations that are close to experimental values. The application of a W_F expression that is not valid for high-carbon, quench-and-tempered steels results in incorrect calculations of σ_C. To the best of the author's knowledge, there is currently no W_F expression that is suitable for high-carbon steels with quench and tempered microstructure. The development of such an expression for W_F, if at all necessary, is a task for future work.

The values for the terms γ_s, ρ, f, and E_{Str} in the modified model are 0.15 J m^{-2}, 3×10^{-5} mol m^{-2}, 0.01, and 500 J mol^{-1}, respectively [11,24]. If martensite transformation is assumed to initiate on the most favourably oriented nuclei, the value of $\frac{\partial \Delta G}{\partial \sigma}$ is −0.86 J mol^{-1} MPa^{-1} when the stress state is in uniaxial tension [25]. This applies to all the steels in the present work since they were subjected to uniaxial tensile tests.

The shape factor α is fitted by using the Curve Fitter app in MATLAB 2022a. The procedure involves defining ΔG^{AW}_{Chem} and V^0_γ as the independent variables, whereas the measured σ_C of the quench-and-tempered steels [4–6] is defined as the dependent variable (under 'Select Data' in the app, set ΔG^{AW}_{Chem}, V^0_γ, and measured σ_C as the 'X Data', 'Y Data', and 'Z Data', respectively). The shape factor α is obtained by fitting these variables into the modified critical stress model (under 'Fit Type' in the app, select the 'Custom Equation' mode and insert Equation (11)), while keeping the values of other parameters (see Table 4) unchanged. This yields a value of 0.7899 (±0.0215) for the shape factor α.

Therefore, the modified critical stress model is expressed as:

$$\sigma_C = \frac{1}{\left(\frac{\partial \Delta G}{\partial \sigma}\right)^{AW}} \cdot \left\{ \frac{2\alpha^{AW} \cdot \gamma_s/\rho}{\ln\left[-\frac{\ln(1-f)}{V^0_\gamma}\right]} - \Delta G^{AW}_{Chem} - E_{Str} \right\}. \quad (11)$$

The parameter values for implementing Equation (11) are summarised in Table 4. Equation (11) has four fixed parameters (γ_s, ρ, f, and E_{Str}) and four free parameters ($\left(\frac{\partial \Delta G}{\partial \sigma}\right)^{AW}$, α^{AW}, V^0_γ, and ΔG^{AW}_{Chem}). Note that the number of free parameters in Equation (7) has been reduced from six to four in Equation (11) by replacing $(N^0_v)^{GH}$and V^{GH}_p with V^0_γ and removing W^{GH}_F. This shows that the modified model requires fewer free parameters to calculate the critical stress of martensite transformation in high-carbon quench-and-tempered steels.

Description of the austenite volume fraction model

The derivation of a model that calculates the volume fraction of retained austenite, V_γ, as a function of applied true stress, σ is presented in this section. Martensite transformation occurs when $\Delta G_{Total} \geq \Delta G_{M_s}^{\gamma \rightarrow \alpha'}$. If the steel is mechanically loaded at a constant temperature, ΔG_{Chem} is assumed to remain constant. The martensitic transformation is solely driven by ΔG_{Mech}, which is a function of σ. For the steels investigated in this work, V_γ was observed to decrease with σ when σ is greater than σ_C [4–6].

If the change in the martensite fraction $dV_{\alpha'}$ for a given increment of σ is proportional to V_γ, then:

$$\frac{dV_{\alpha'}}{d\sigma} = KV_\gamma, \tag{12}$$

where K is a constant.

Since $V_{\alpha'} = V_\gamma^0 - V_\gamma$, integration of Equation (12) gives:

$$\ln V_\gamma - \ln V_\gamma^0 = K\sigma. \tag{13}$$

Equation (13) can be expressed as

$$V_\gamma = V_\gamma^0 \cdot exp[K \cdot (\sigma - \sigma_C)], \tag{14}$$

where

$$V_\gamma = V_\gamma^0 if \sigma \leq \sigma_C.$$

Since retained austenite starts transforming only when σ is greater than σ_C, the V_γ when $\sigma \leq \sigma_C$ is set to be equal to V_γ^0. The term K (MPa^{-1}) represents the slope of the function and is fitted by plotting the experimental values of $\ln V_\gamma - \ln V_\gamma^0$ versus $(\sigma - \sigma_C)$ for the linear, decreasing segment of the experimental transformation curves [4–6]. The values of K for 8620, 4320, 3310, A485-M1, and 52100-QT steels are -4.948×10^{-4}, -5.108×10^{-4}, -5.389×10^{-4}, -7.307×10^{-4}, and -6.09×10^{-4} MPa^{-1}, respectively. A value of $K = -5.768 \times 10^{-4}$ is obtained from the average of the K values of these steels, and this value is applied in subsequent calculations using Equation (14).

Determination of σ_C and V_γ from experimental data

The experimental values of σ_C and V_γ are determined from the retained austenite volume fraction and true stress measured during the uniaxial tensile tests of the steels. These tests were performed using neutron diffraction (for 8620, 4320, 3310, and A485-M1 steels) and synchrotron XRD (for 52100-QT steel). The models were validated with measured σ_C and V_γ from experimental datasets provided by the respective authors [4,5] for the first group of steels, while the experimental σ_C and V_γ values for 52100-QT steel were obtained by digitising the results reported in [6].

The authors in [4–6] did not define a procedure for determining σ_C from the transformation curves. Therefore, the selection of σ_C was arbitrary and most likely corresponds to the highest value of V_γ before an apparent decrease in V_γ was observed. The same approach was adopted to determine σ_C from the experimental datasets of the steels in the present study.

Results

Calculated σ_C for steels with quench-and-tempered microstructures

The calculations of σ_C are performed according to the original and modified critical stress models. Values of the model parameters are described in Tables 3 and 4.

Table 5 shows the experimentally measured and calculated σ_C for the quench-and-tempered steels as mentioned in Table 1. The σ_C values calculated using Equation (7) are significantly higher than the measured values for the respective steels, whereas the calculated values from Equation (11) are closer to the measured values. The difference between measured and calculated σ_C values for the 8620, 4320, and 3310 steels are within $\pm$ 45 MPa, whereas those for the A485-M1 and 52100-QT steels are within $\pm$ 345 MPa. Despite the differences, Equation (11) performs better than Equation (7) in calculating σ_C for quench-and-tempered high-carbon steels.

Calculated σ_C for steels with alternative microstructures

The application of Equation (11) in steels with other microstructures is assessed by calculating the σ_C for bainitic and quench-and-partitioning (QP) steels. According to Table 6, the steels are labelled according to their respective designations in [7] (for A485 steel) and [6] (for 52100 steel). The heat treatments of these steels are described in [6,7]. The σ_C is calculated with Equation (11) according to the procedure described in Section 3.3. The C_γ for the steels is calculated with Equation (1). The concentrations of the other alloying elements are assumed to follow the respective compositions of the A485-M1 and 52100-QT steels in Table 1.

Table 6 shows the measured and calculated σ_C values for bainitic and QP steels. When comparing the steels subjected to the same type of heat treatment (i.e. A485-B1/B2; 52100-B220/240/260; 52100-QP220/240), the measured and calculated σ_C values increase when the magnitude of ΔG_{Chem} is smaller and when V_γ^0 decreases. Despite the ability of the model to correctly predict the variation of σ_C with V_γ^0 and ΔG_{Chem}, the differences between the measured and calculated σ_C

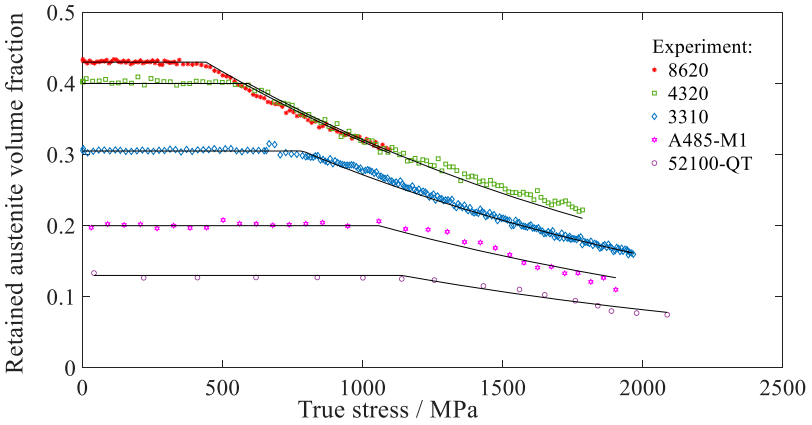

Figure 1. Measured and calculated retained volume fraction (V_γ) of steels with quench-and-tempered microstructure.

values are large — on the order of ±135–800 MPa. Possible reasons are discussed in Section 7.1.

Calculated V_γ for steels with quench-and-tempered microstructures

Figure 1 shows the variation of V_γ with the measured true stress of the quench-and-tempered steels [4–6], where V_γ is calculated with Equation (14). The region of mechanical stability is indicated by the portion of the curve where V_γ remains constant. The transition point on the curve represents the onset of martensite transformation when $\sigma > \sigma_C$. A comparison of the curves shows that the transformation initiates at later stages as σ_C becomes higher. Based on Figure 1, 52100-QT has the highest σ_C and, therefore, the most mechanically stable retained austenite among the quench-and-tempered steels. The curves predicted by Equation (14) agree well with the experimental data.

Calculated V_γ for steels with alternative microstructures

The utility of Equation (14) is assessed by calculating the V_γ for the bainitic and QP steels described in Section 6.2. The calculation is performed by setting σ_C according to the measured σ_C values of the respective steels in Table 6. The model is also applied to predict the transformation curve for a TRIP steel that was tensile-tested at 293 K [8]. Since the TRIP steel showed immediate retained austenite transformation upon loading, V_γ is calculated by setting σ_C as 0 in Equation (14). Based on the transformation curves shown in Figure 2, the V_γ calculated with Equation (14) show good agreement with the experimental data.

Discussion

Critical stress for retained austenite to martensite transformation

Referring to Table 6, steels subjected to the same type of heat treatment (i.e. A485-B1/B2, 52100-B220/240/260, and 52100-QP220/240) exhibit higher σ_C values when the magnitude of ΔG^{AW}_{Chem} is smaller. The physical meaning of a smaller magnitude of ΔG^{AW}_{Chem}, i.e. lower chemical driving force, is that the retained austenite is more resistant towards martensite transformation, which is caused by a higher C_γ. This indicates a higher retained austenite stability which means that the martensite transformation initiates at a higher σ_C.

The σ_C is also observed to increase with a lower V^0_γ. However, it is challenging to analyse the effect of V^0_γ on the calculation of σ_C separately from chemical composition effects. The A485-M1 and 52100-QT steels are considered as an example. Although both steels have very similar C_γ (see Table 1), the magnitude of the ΔG^{AW}_{Chem} for 52100-QT is 149 J mol^{-1} higher than that of A485-M1 steel, presumably due to the effect of other alloying elements on the chemical driving force. If the critical stress is considered only on the basis of chemical composition via the chemical driving force, then the σ_C of 52100-QT steel is expected to be lower than that of A485-M1 steel because of lower retained austenite stability.

However, the measured σ_C of 52100-QT (1140 MPa) is higher than that of A485-M1 (1058 MPa). This is most likely because the 52100-QT steel has a lower V^0_γ than the A485-M1 steel, which corresponds to a higher amount of martensite in the microstructure before the steel was mechanically loaded.

According to Xiong et al. [17], the martensite plates, which have a higher yield stress than austenite, could obstruct the retained austenite grains from transforming into martensite. This occurs because the martensite matrix surrounding the grains must deform to contain the volume expansion caused by martensitic transformation [17]. They also proposed that the hydrostatic pressure induced by the residual stress generated in the microstructure could hinder martensite transformation, which is accompanied by volume expansion.

Since V^0_γ replaces the product $(N^0_v)^{GH} \cdot V^{GH}_p$ in the critical stress model, the term V^0_γ collectively represents the number density of martensitic nucleation sites and austenite particle volume. The physical meaning

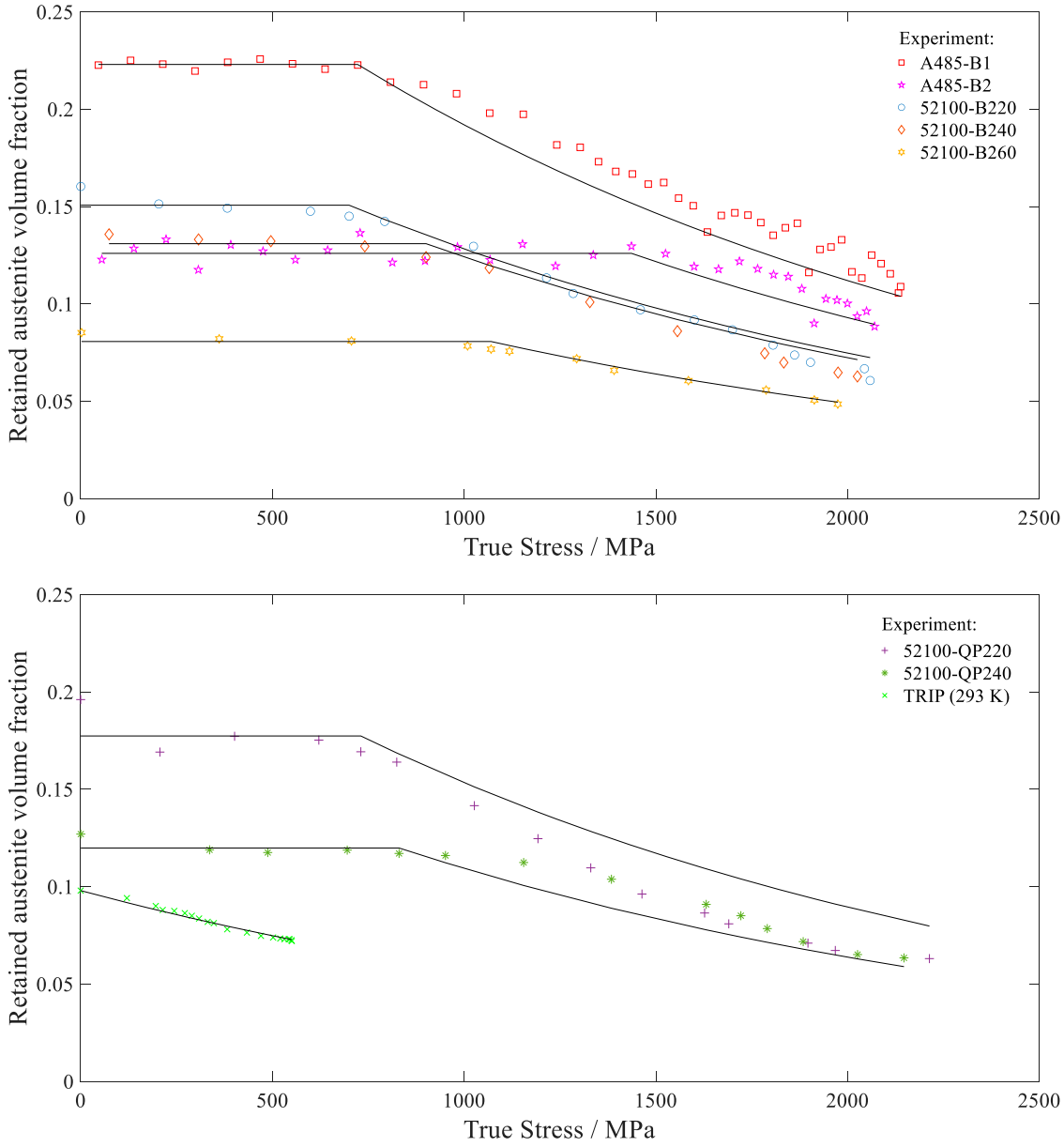

Figure 2. Measured and calculated retained austenite volume fraction (V_γ) of bainitic, QP and TRIP steels. The transformation curves are shown in separate plots for clarity.

of this representation is that a lower V_γ^0 indicates lesser martensitic nucleation sites so that the martensite transformation is triggered and detected at a higher σ_C.

These reasons could explain why 52100-QT has a higher σ_C than A485-M1 because of a lower V_γ^0, an effect that is reflected by the modified critical stress model.

In Table 6, major differences are observed between the measured and calculated σ_C values for bainitic and QP steels. Bainite is reported to dominate the bainitic and QP microstructures of the corresponding A485 [33] and 52100 [6] steels. Therefore, the large differences in σ_C are most likely a result of the influence of bainite on the load partitioning behaviour; thus, its subsequent effect on austenite stability is not considered in the modified critical model.

When a composite microstructure containing phases of variable properties is stressed, the soft phase that is more ductile is the first to deform plastically. The deformation is followed by work hardening. The load will be eventually transferred to the harder phase [34]. Therefore, in a microstructure containing phases of varying strengths, the critical transformation stress of retained austenite also depends on the mechanical response of the surrounding phases when deformation is applied.

Referring to a study on austenite stability and strain evolution in TRIP-assisted steels as an example [35], the matrix composed of ferrite and bainitic ferrite was found to have the lowest load-bearing capacity, followed by austenite and martensite. The authors also reported that the transformation of austenite into martensite in the steel with more bainitic ferrite

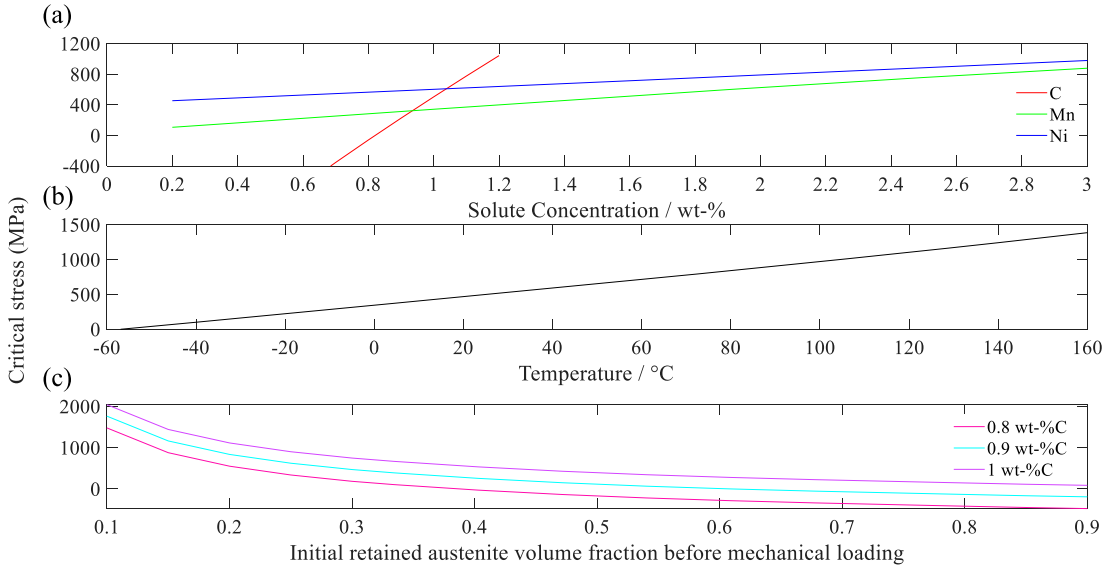

Figure 3. The change in critical stress σ_C as a function of (a) solute concentration; (b) temperature; (c) V_γ^0.

occurred at later stages of the deformation due to delayed work-hardening of the matrix microstructure [35]. These observations can be related to the relative strengths of the phases present in the microstructure [36].

According to the work of Foster et al. [6], the σ_C increases with C_γ and the amount of bainitic ferrite in the steels with bainitic (i.e. 52100-B) and QP (i.e. 52100-QP) microstructures. However, these steels have a lower σ_C than the 52100-QT steel, which has a tempered martensite microstructure. The varying austenite stabilising effects conferred by these different matrices were attributed to the presence of nano-carbides and local straining of the bainitic ferrite surrounding the austenite grains [6]. These observations point to the major effect of the surrounding matrix on austenite stability.

Currently, the modified critical stress model does not consider explicitly the austenite stabilising effect of the surrounding matrix microstructure. Since the model parameters are fitted based on the composition and microstructure of tempered martensitic steels, the σ_C calculated with the modified model is expected to differ significantly from the measured σ_C of steels with other microstructures. The incorporation of the austenite stabilising effects by the surrounding matrix in relation to some of the aforementioned factors is considered for future work on the critical stress model.

Kinetics of deformation-induced martensite transformation

Based on the measured and predicted V_γ as shown in Figures 1 and 2, the application of Equation (14) appears to work for all steel microstructures in the current investigation. However, the model may underestimate (e.g. for A485-B1 steel in Figure 2) or overestimate (e.g. for 52100-QP220 steel in Figure 2) V_γ during retained austenite transformation. This is because the average K value as mentioned in Section 4, i.e. $K = -5.768 \times 10^{-4}$, is applied in all calculations, which may be slightly different from the K value obtained from each dataset.

Nonetheless, the model predictions are in good agreement with measured values, demonstrating that the model can predict the retained austenite fraction for stress-induced martensite transformations in the investigated steels regardless of whether the steel exhibits a delayed transformation of retained austenite.

Parametric analysis of the critical stress model

To determine the constraints of the critical stress model, the influences of ΔG_{Chem}^{AW} and V_γ^0 on σ_C are examined. A parametric analysis of Equation (11) is conducted by calculating the σ_C of 8620 steel (see Table 1) across a range of ΔG_{Chem}^{AW} and V_γ^0 values while keeping the other parameters constant.

Since ΔG_{Chem}^{AW} changes with chemical composition, the effect of chemical composition is assessed by calculating σ_C across a range of concentrations for the austenite stabilisers (carbon, manganese, and nickel) at a constant temperature of 20°C and V_γ^0 of 0.43. Based on Figure 3(a), the σ_C increases with higher concentrations of carbon, manganese, and nickel. The austenite stabilising effect of these elements raises the free energy required to initiate martensite transformation. Since $\Delta G_{Total} \geq \Delta G_{M_s}^{\gamma \rightarrow \alpha'}$ to initiate martensite transformation, a higher ΔG_{Mech} is needed, which is indicated by a higher σ_C. Furthermore, the rate of increase in σ_C per wt-% alloying element is highest for carbon, followed by manganese and then nickel. This observation agrees with the reported austenite stabilising potencies of these elements [37], where carbon is known to be the

strongest austenite stabiliser, followed by manganese and nickel.

The effect of temperature on σ_C is studied by calculating σ_C at −60°C–160°C, according to the chemical composition of 8620 steel and a V_γ^0 of 0.43. The selected temperature range is based on standard service temperatures for bearings [38]. The martensite transformation is less likely to occur at elevated temperatures because there is less undercooling available to provide the required thermodynamic driving force through ΔG_{Chem}. Thus, σ_C increases with temperature (as shown in Figure 3(b)) because a higher ΔG_{Mech} is needed to supplement the driving force for martensite transformation.

This observation agrees with the experimental findings of Neu and Sehitoglu [39]. By performing uniaxial tensile tests on carburised 4320 steel across a temperature range of −60°C–50°C, the authors reported decreasing transformation amounts with higher testing temperatures and speculated that little stress-induced retained austenite transformation occurs above 60°C [39].

The experimental findings of Kulin et al. [40] also demonstrated that stress-induced transformation decreases as the testing temperature increases progressively above the M_s temperature of a 0.5C-20Ni (wt-%) steel (assumed to be −37°C). They reported that martensite transformation was barely observed at 0°C and non-existent at 20°C, showing that the stress-induced transformation occurred within a narrow range between the M_s temperature and approximately 40°C above the M_s. Based on the M_s equation developed by Bohemen [41], the M_s temperature of the 8620 steel is calculated to be approximately 136°C. Thus, it could be implied that minimal or no stress-induced transformation would occur in 8620 steel at testing temperatures higher than 136°C.

The variation of σ_C with V_γ^0 is evaluated by calculating the σ_C of 8620 steel at a temperature of 20°C and setting C_γ to 0.8, 0.9, and 1 wt-%C, respectively. The concentrations of other alloying elements follow that of 8620 steel in Table 1. According to Figure 3(c), the σ_C increases with C_γ at a constant V_γ^0. When C_γ is constant, the σ_C decreases with increasing V_γ^0. This trend is consistent with the measured σ_C of the quench-and-tempered steels (Table 5) with respect to their V_γ^0 (Table 4), where 8620 steel has the lowest measured σ_C of 441 MPa but the highest V_γ^0 of 0.43. In Table 6, steels subjected to the same type of heat treatment also showed higher σ_C with lower V_γ^0. The observation that a higher retained austenite fraction leads to lower critical stress for martensite transformation agrees with the findings of Alley and Neu [9]; the authors described the variation of σ_c with V_γ^0 through an empirical equation.

Strictly speaking, the relationship between σ_C and V_γ^0 is linked to the chemical composition and heat treatment of the steel. Considering the 52100 bainitic steels in Table 6 (B220/240/260) as an example, the increasing bainitic treatment temperatures result in higher amounts of austenite decomposing into bainite [6], as the remaining austenite becomes enriched with carbon due to carbon partitioning [34]. This leads to a lower V_γ^0 and higher C_γ, thus increasing the stability of the austenite as indicated by a higher σ_C. Zhou et al. [42] reported high retained austenite mechanical stability during tensile testing of a medium-manganese steel with low V_γ^0 that contained a high solute concentration and small grain size, which is a consequence of heat treatment.

Despite the good agreement between experimental trends and σ_C values predicted by Equation (11), the model has its limitations. The main constraint of the model is the range of chemical composition and V_γ^0 values that were used to develop the model parameters. Consequently, the model predicts negative σ_C values in certain conditions: below 0.8 wt-%C (Figure 3(a)); at temperatures below −60°C (Figure 3(b)); above $V_\gamma^0 = 0.35$ when $C_\gamma = 0.8$ wt-%C; and above $V_\gamma^0 = 0.6$ when $C_\gamma = 0.9$ wt-%C (Figure 3(c)).

Equation (11) predicts a negative σ_C value when ΔG_{Chem} is greater in magnitude than the energy barrier to martensite transformation, which is defined in the terms $\frac{2\alpha^{AW}\cdot\gamma_s/\rho}{\ln\left[-\frac{\ln(1-f)}{V_\gamma^0}\right]}$ and E_{Str}. This could imply that the delayed deformation-induced transformation of retained austenite into martensite does not occur or occurs shortly after mechanical loading. The latter scenario applies to low-carbon TRIP steels [8]; in this case, the critical stress model of Haidemenopoulos et al. [11] might provide better predictions of σ_C.

Another reason for the prediction of a negative σ_C is because the same value of α (0.7899) is applied in all calculations. The value of α was previously reported to be 0.866 by Haidemenopoulos et al. [10,11]. However, Olson et al. [27] reported a value of $\alpha = 0.84$, which they obtained by best-fitting Equations (2) and (5). In the process of fitting α for the quench-and-tempered steels, it was found that α is sensitive to carbon content. A lower α value results in reasonable predictions of σ_C when C_γ is lower than the current threshold of 0.8 wt-%C (see Figure 3(a)).

This observation agrees with recent work by Haidemenopoulos et al. [21] and Polatidis et al. [30] on low-carbon TRIP steels, where a value of 0.1 was used for the shape factor α. Haidemenopoulos et al. [21] reported that the value of α should be lower for steels with retained austenite that is less stable. Referring to Equation (5), a low value of α results in high N_v, which implies a higher density of potent martensitic nucleation sites. N_v is dependent on the potency of martensitic nucleation site n, which explains why it is appropriate to use a low α value to predict σ_C for

retained austenite grains with low stability, such as those with low-carbon content. Inversely, the value of α is expected to be higher when predicting σ_C for retained austenite grains with higher stability, as is the case with the high-carbon steels in the present investigation.

The utility of Equation (11) can be extended by assessing the mechanical stability of the retained austenite in high-carbon steels in other stress states. For example, retained austenite in a case-carburised steel has been reported to transform into martensite under rolling contact fatigue (RCF) conditions [43]. The $\frac{\partial \Delta G}{\partial \sigma}$ parameter in Equation (11) should be modified accordingly when the stress state is different.

The parametric analysis of Equation (11) showed that σ_C increases with higher austenite stabiliser (carbon, manganese, nickel) concentrations, higher temperatures, and lower V_γ^0. While the effects of these parameters on σ_C have been assessed separately, they are interrelated in practice and should be considered collectively when the model is implemented. The analysis also identified α as a limiting factor for the application of this model, as it is expected to change with other steel compositions and V_γ^0. Despite the model constraints as imposed by the composition and experimental conditions of the quench-and-tempered steels, this model can be extended to other steels by deriving the relevant material parameters following the procedures outlined in Section 3.

Model applications

Potential applications for the critical stress and austenite volume fraction models are explored in this section. Previous research has indicated that higher amounts of retained austenite increase the RCF life of bearings [1,2]. On the contrary, Morris and Sadeghi [43] have reported that higher amounts of retained austenite do not automatically improve the RCF life of bearings; the underlying reason is that the high stability of retained austenite restricts its transformation into martensite when subjected to RCF stresses. They found that the benefits of retained austenite to the improvement of RCF life, regardless of its amount, are realised only when its stability is below a threshold that allows martensite transformation during deformation.

Since σ_C can be used as an indicator of retained austenite mechanical stability, the following examples highlight the implementation of Equations (11) and (14) in selecting chemical compositions and processing parameters for alloy design.

The first example explores different alloy compositions for defined ranges of σ_C. By setting a temperature

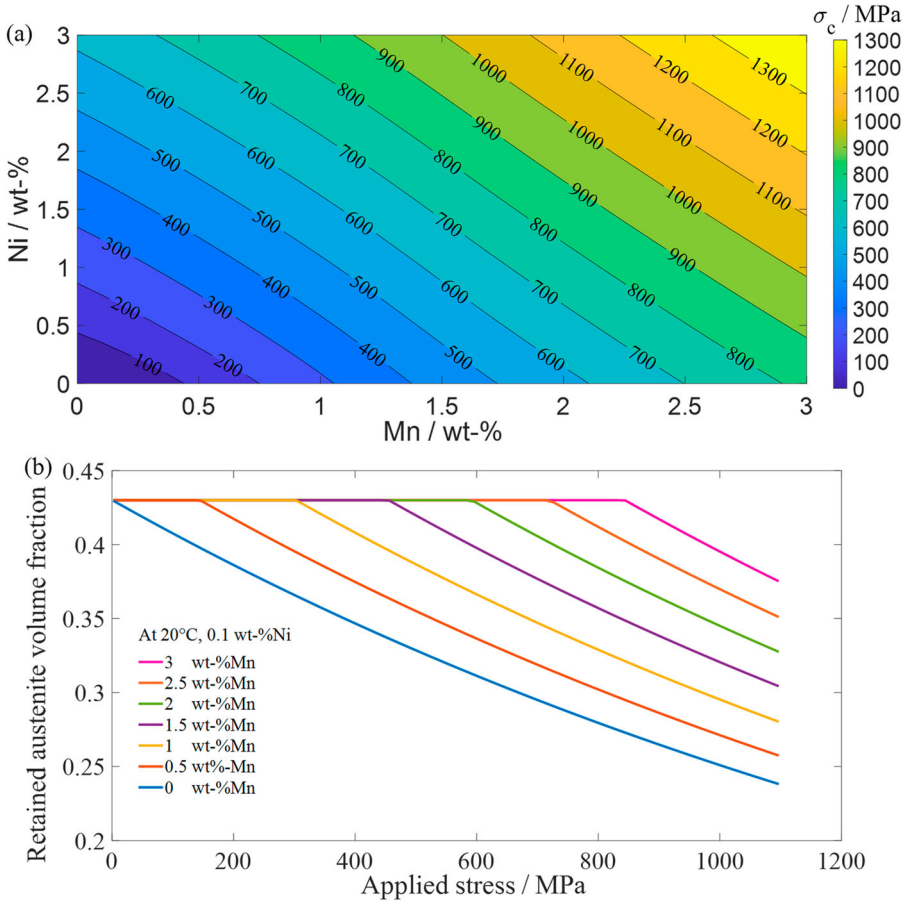

Figure 4. (a) Required manganese and nickel concentrations for a range of critical stresses at a deformation temperature of 20°C and V_γ^0 of 0.43; (b) change in retained austenite volume fraction (V_γ) with applied stress for selected compositions.

of 20°C and V_γ^0 of 0.43, σ_C is calculated within a composition range of 0–3 wt-%Mn and 0–3 wt-%Ni, in steps of 0.1 wt-% Mn/Ni. The concentrations of carbon and other alloying elements follow that of 8620 steel (see Table 1). Figure 4(a) shows the required manganese-nickel combinations in austenite as σ_C is varied, in which higher concentrations of manganese and nickel increase σ_C.

To illustrate how variation in the CALPHAD calculations, e.g. by Thermodynamic database accuracy, could affect the model calculations, a sensitivity analysis is conducted, via minor changes in the chemical composition to estimate model variations. When the manganese concentration is set as 1.4 wt% in 8620, the calculated σ_C for nickel concentrations of 0, 0.2, 0.4, 0.6, 0.8, 1, 1.2, and 1.4 wt-% are 407, 445, 482, 519, 556, 594, 631, and 669 MPa, respectively. When the nickel concentration is set as 1.4 wt-%, the calculated σ_C for manganese concentrations of 0, 0.2, 0.4, 0.6, 0.8, 1, 1.2, and 1.4 wt-% are 311, 355, 403, 453, 505, 558, 612, and 669 MPa, respectively. The results demonstrate a model sensitivity of $\sim$200–220 MPa/wt% for σ_C, indicating relatively low sensitivity to possible changes in the CALPHAD predictions, given the narrow range in compositional differences in high-carbon steels ($<$ 1–2 wt%, Table 1) and the accuracy in the predicted results in Table 5 for several steels. Further assessment on the accuracy of the CALPHAD calculations is beyond the scope of the present work.

In bearing applications, the chemical composition should be selected to ensure that retained austenite remains stable at the applied loads during service. Figure 4(a) can be used as a guide to select suitable alloy compositions for a defined range of σ_C. Since the price of manganese is lower than nickel [44], using a high manganese-low nickel combination may make it possible to manufacture bearings at significantly lower prices than those alloys in current use.

Figure 4(b) shows the stress-induced transformation progress of retained austenite for various manganese concentrations when the deformation temperature and nickel concentration are fixed at 20°C and 0.1 wt-%, respectively. As the manganese concentration increases, martensite transformation initiates at higher σ_C values and a higher amount of retained austenite is left when the stress is removed. Figure 4(b) can be used to inform the selection of manganese-nickel combinations that optimise martensite transformation (i.e. the 'TRIP effect') and to control the amount of retained austenite; this is useful in metal forming operations.

The second example explores different alloy compositions for a defined range of σ_C at various deformation temperatures. Setting V_γ^0 as 0.43 and following the composition of 8620 steel, the calculation is performed within a temperature range of −50°C–80°C in steps of 10°C and 0.05 wt-% Mn/Ni. The calculation is also constrained to compositions that result in σ_C between 400 and 500 MPa (noting that the measured σ_C of 8620 steel is 441 MPa). According to Figure 5(a), the concentrations of manganese and nickel required to achieve σ_C within the target range increase with lower deformation temperatures. Since retained austenite transforms more easily into martensite at low temperatures due to greater undercooling, a higher concentration of austenite stabilisers is needed to maintain austenite stability.

It was found that σ_C exceeds 500 MPa when the deformation temperature is above 80°C. Figure 5(b) shows the changes in V_γ with σ at different temperatures. The composition is set as 0.3Mn-1.4Ni (wt-%) because this combination is closest to that of 8620 steel (see Table 1). As temperature increases, martensite transformation occurs at higher critical stresses with lesser retained austenite remaining after the stress is removed; no transformation occurs at 120°C. Considering the service temperature range for most rolling-element bearings (i.e. ranging from −50°C up to the order of 120–150°C) [38], the dimensional stability of bearings is critical as fluctuations in service temperature can induced retained austenite decomposition. Therefore, the information from the calculations shown in Figure 5 can aid the design of bearing compositions that optimise retained austenite stability against the transformation induced by temperature fluctuations, which is crucial for bearings operating in extreme environments.

The examples have shown the utility of the models in predicting the parameters for optimal austenite stability in bearing applications once a target stress and/or strain are defined. However, the influence of heat treatments and manufacturing processes should also be considered, as the models do not explicitly account for these factors. For instance, while it is known that manganese can promote austenite stability as well as nickel but with higher cost-effectiveness, excessive amounts of manganese can cause surface and internal oxidation in carburised steels [45]. Therefore, these models should be implemented together with other manufacturing considerations to inform the design process of new bearings.

Conclusions

In this work, models for predicting the critical stress and progress of deformation-induced martensite transformation in high-carbon steels have been developed. The critical stress model (Equation (11)) was developed to overcome the limitations of existing models when predicting σ_C in high-carbon quench and tempered steels, which exhibit delayed retained austenite transformation under applied stress. Compared to

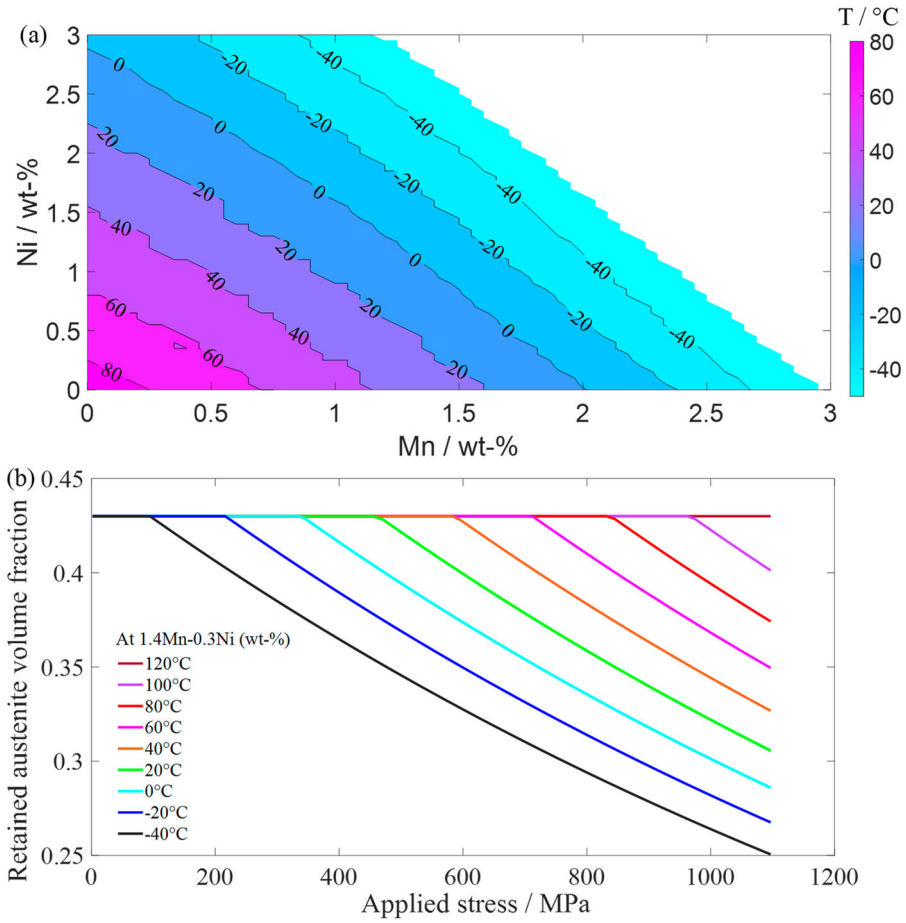

Figure 5. (a) Required manganese and nickel concentrations for deformation temperatures between −50°C and 80°C with σ_C values within a range of 400–500 MPa; (b) change in retained austenite volume fraction (V_γ) with applied stress for a composition of 1.4Mn-0.3Ni (wt-%) within a temperature range of −40°C to 120°C.

Equation (7), i.e. the model of Haidemenopoulos et al. [10], Equation (11) requires fewer free parameters (i.e. reduced from six to four), providing better physical and numerical interpretations in the parameter selection and reduction to study TRIP in high-carbon steels. Calculations of σ_C with Equation (11) are in good agreement with measured values from the investigated quench-and-tempered steels.

Equation (11) considers the influence of chemical composition, deformation temperature, and initially retained austenite fraction on σ_C. Higher austenite stabiliser concentrations in the composition or higher deformation temperatures result in austenite that is more stable against transformation; these effects are represented by a smaller magnitude of ΔG_{Chem}. A lower V_γ^0 indicates fewer martensitic nucleation sites, which means that the martensite transformation under applied stress occurs at a higher σ_C.

Since the critical stress model was developed based on steels with microstructures that consist primarily of tempered martensite and retained austenite, the accuracy of the model predictions diminishes when applied to steels with other microstructures. In contrast, the model for calculating the transformed amounts of retained austenite under applied stress (Equation (14)) was found to perform well when applied to steels that exhibit (i.e. high-carbon steels) or do not exhibit (i.e. low-carbon steels) the delayed retained austenite transformation phenomenon.

A parametric analysis of Equation (11) showed that σ_C increases with higher austenite stabiliser concentrations, higher deformation temperatures, and lower V_γ^0. Besides identifying the limiting conditions of the model, the analysis highlighted the sensitivity of the shape factor α to material parameters, notably C_γ. Potential model applications have been explored. It is anticipated that these models can be used to aid the design of new alloy compositions for bearings with optimal retained austenite stability and cost-effectiveness.

Acknowledgements

Adriel Wong gratefully acknowledges the financial support provided by The Timken Company for this work as part of a PhD project. Enrique Galindo-Nava acknowledges funding from RAEng in the form of a research fellowship.

Disclosure statement

No potential conflict of interest was reported by the authors.

Funding

This work was supported by Royal Academy of Engineering.

References

[1] Dommarco RC, Kozaczek KJ, Bastias PC, et al. Residual stresses and retained austenite evolution in SAE 52100 steel under non-ideal rolling contact loading. Wear. 2004;257:1081–1088.
[2] Shen Y, Moghadam SM, Sadeghi F, et al. Effect of retained austenite–compressive residual stresses on rolling contact fatigue life of carburized AISI 8620 steel. Int J Fatigue. 2015;75:135–144.
[3] Sidoroff C, Perez M, Dierickx P, et al. Advantages and shortcomings of retained austenite in bearing steels: A review, Bearing Steel Technologies: 10th Volume, Advances in Steel Technologies for Rolling Bearings. (2015).
[4] Bedekar V, Voothaluru R, Yu D, et al. Effect of nickel on the kinematic stability of retained austenite in carburized bearing steels – In-situ neutron diffraction and crystal plasticity modeling of uniaxial tension tests in AISI 8620, 4320 and 3310 steels. Int J Plast. 2020;131:1–16.
[5] Voothaluru R, Bedekar V, Xie Q, et al. In-situ neutron diffraction and crystal plasticity finite element modeling to study the kinematic stability of retained austenite in bearing steels. Mater Sci Eng A. 2018;711:579–587.
[6] Foster D, Paladugu M, Hughes J, et al. Comparative micromechanics assessment of high-carbon martensite/bainite bearing steel microstructures using in-situ synchrotron X-ray diffraction. Materialia (Oxf). 2020;14:100948.
[7] Voothaluru R, Bedekar V, Yu D, et al. Investigating the difference in mechanical stability of retained austenite in bainitic and martensitic high-carbon bearing steels using in situ neutron diffraction and crystal plasticity modeling. Metals (Basel). 2019;9:482–498.
[8] Blondé R, Jimenez-Melero E, Zhao L, et al. High-energy X-ray diffraction study on the temperature-dependent mechanical stability of retained austenite in low-alloyed TRIP steels. Acta Mater. 2012;60:565–577.
[9] Alley ES, Neu RW. A hybrid crystal plasticity and phase transformation model for high carbon steel. Comput Mech. 2013;52:237–255.
[10] Haidemenopoulos GN, Vasilakos AN. On the thermodynamic stability of retained austenite in 4340 steel. J Alloys Compd. 1997;247:128–133.
[11] Haidemenopoulos GN, Vasilakos AN. Modelling of austenite stability in low-alloy triple-phase steels. Steel Res. 1996;67:513–519.
[12] Behera AK, Olson GB. Prediction of carbon partitioning and austenite stability via non-equilibrium thermodynamics in Quench and Partition (Q&P) steel. JOM. 2019;71:1375–1385.
[13] Haidemenopoulos GN, Grujicic M, Olson GB, et al. Thermodynamics-based alloy design criteria for austenite stabilization and transformation toughening in the Fe-Ni-Co system. J Alloys Compd. 1995;220:142–147.
[14] Olson GB, Cohen M. Kinetics of strain-induced martensitic nucleation. Metall Trans A. 1975;6A:791–795.
[15] Das A, Chakraborti PC, Tarafder S, et al. Analysis of deformation induced martensitic transformation in stainless steels. Mater Sci Technol. 2011;27:366–370.
[16] Tamura I. Deformation-induced martensitic transformation and transformation-induced plasticity in steels. Met Sci. 1982;16:245–253.
[17] Xiong XC, Chen B, Huang MX, et al. The effect of morphology on the stability of retained austenite in a quenched and partitioned steel. Scr Mater. 2013;68:321–324.
[18] Hidalgo J, Findley KO, Santofimia MJ. Thermal and mechanical stability of retained austenite surrounded by martensite with different degrees of tempering. Mater Sci Eng A. 2017;690:337–347.
[19] Jacques PJ, Delannay F, Ladrière J. On the influence of interactions between phases on the mechanical stability of retained austenite in transformation-induced plasticity multiphase steels. Metall Mater Trans A. 2001;32:2759–2768.
[20] Bhadeshia H. Steels for bearings. Prog Mater Sci. 2012;57:268–435.
[21] Haidemenopoulos GN, Aravas N, Bellas I. Kinetics of strain-induced transformation of dispersed austenite in low-alloy TRIP steels. Mater Sci Eng A. 2014;615:416–423.
[22] Olson GB. Effects of stress and deformation on martensite formation. In: K Buschow, R Cahn, M Flemings, B Ilschner, E Kramer, S Mahajan, P Veyssière, editor. Encyclopedia of materials: science and technology. Oxford: Elsevier; 2001. p. 2381–2384.
[23] Olson GB, Cohen M. A general mechanism of martensitic nucleation: part I. General concepts and the FCC → HCP transformation. Metall Trans A. 1976;7:1897–1904.
[24] Olson GB, Cohen M. A general mechanism of martensitic nucleation: part II. FCC → BCC and other martensitic transformations. Metall Trans A. 1976;7:1905–1914.
[25] Olson GB, Cohen M. Stress-assisted isothermal martensitic transformation: application to TRIP steels. Metall Trans A. 1982;13:1907–1914.
[26] Cohen M, Olson GB. Martensitic nucleation and the role of the nucleating defect, in: First JIM International Symposium on New Aspects of Martensitic Transformation, Suppl. to Trans. JIM, Japan Institute of Metals, 1976: pp. 93–98.
[27] Olson GB, Tsuzaki K, Cohen M. Statistical aspects of martensitic nucleation. MRS Proceedings. 1985;57:129.
[28] Cech RE, Turnbull D. Heterogeneous nucleation of the martensite transformation. JOM. 1956;8:124–132.
[29] Samek L, de Moor E, Penning J, et al. Influence of alloying elements on the kinetics of strain-induced martensitic nucleation in low-alloy, multiphase high-strength steels. Metall Mater Trans A. 2006;37:109–124.
[30] Polatidis E, Haidemenopoulos GN, Krizan D, et al. The effect of stress triaxiality on the phase transformation in transformation induced plasticity steels: experimental investigation and modelling the transformation kinetics. Mater Sci Eng A. 2021;800:140321.
[31] Andersson JO, Helander T, Höglund L, et al. Thermo-Calc and DICTRA, computational tools for materials science. CALPHAD. 2002;26:273–312.
[32] Ghosh G, Olson GB. Kinetics of FCC→ BCC heterogeneous martensitic nucleation—I. The critical driving force for athermal nucleation. Acta Metall Mater. 1994;42:3361–3370.

[33] Voothaluru R, Bedekar V, Yu D, et al. Investigating the difference in mechanical stability of retained austenite in bainitic and martensitic high-carbon bearing steels using in situ neutron diffraction and crystal plasticity modeling. Metals (Basel). 2019;9:482.
[34] Bhadeshia HKDH. Bainite in steels: theory and practice. 3rd ed. London: CRC Press; 2015.
[35] Yan K, Liss K, Timokhina I, et al. In situ synchrotron X-ray diffraction studies of the effect of microstructure on tensile behavior and retained austenite stability of thermo-mechanically processed transformation induced plasticity steel. Mater Sci Eng A. 2016;662:185–197.
[36] Jacques PJ. Transformation-induced plasticity for high strength formable steels. Curr Opin Solid State Mater Sci. 2004;8:259–265.
[37] Totten GE. Steel heat treatment: metallurgy and technologies. 1st ed. Boca Raton: CRC Press; 2006.
[38] Burrier H. Bearing steels. In: Properties and selection: irons, steels, and high-performance alloys. Vol. 1, ASM Handbook, By ASM Handbook Committee. Materials Park, OH: ASM International; 1990. p. 380–388.
[39] Neu RW, Sehitoglu H. Stress-induced transformation in a carburized steel—experiments and analysis. Acta Metall Mater. 1992;40:2257–2268.
[40] Kulin SA, Cohen M, Averbach BL. Effect of applied stress on the martensitic transformation. JOM. 1952;4:661–668.
[41] van Bohemen SMC. Bainite and martensite start temperature calculated with exponential carbon dependence. Mater Sci Technol. 2012;28:487–495.
[42] Zhou TP, Wang CY, Wang C, et al. Austenite stability and deformation-induced transformation mechanism in cold-rolled medium-Mn steel. Mater Sci Eng A. 2020;798:140147.
[43] Morris D, Sadeghi F. Retained austenite stability on rolling contact fatigue performance of 8620 case-carburized steel. Fatigue Fract Eng Mater Struct. 2022;45:55–68.
[44] Choi J, Lee S, Park Y, et al. High manganese austenitic steel for cryogenic applications, in: The Twenty-Second International Offshore and Polar Engineering Conference, OnePetro, 2012.
[45] Krauss G. Microstructures and properties of carburized steels. Heat Treat Irons Steels. 2014;4D:76–87.